Ocean Systems Engineering, *Vol. 8, No. 3 (2018) 281-312*
DOI: https:// doi.org/10.12989/ose.2018.8.3.281

Wind spectral characteristics on strength design of floating offshore wind turbines

Ikpoto E. Udoh* and Jun Zou

Houston Offshore Engineering / Atkins, a member of the SNC-Lavalin Group, 17220 Katy Freeway, Suite 200, Houston, TX 77094, USA

(Received July 18, 2018, Revised August 9, 2018, Accepted August 12, 2018)

Abstract. Characteristics of a turbulence wind model control the magnitude and frequency distribution of wind loading on floating offshore wind turbines (FOWTs), and an in-depth understanding of how wind spectral characteristics affect the responses, and ultimately the design cost of system components, is in shortage in the offshore wind industry. Wind spectrum models as well as turbulence intensity curves recommended by the International Electrotechnical Commission (IEC) have characteristics derived from land-based sites, and have been widely adopted in offshore wind projects (in the absence of site-specific offshore data) without sufficient assessment of design implications. In this paper, effects of wind spectra and turbulence intensities on the strength or extreme responses of a 5 MW floating offshore wind turbine are investigated. The impact of different wind spectral parameters on the extreme blade loads, nacelle accelerations, towertop motions, towerbase loads, platform motions and accelerations, and mooring line tensions are presented and discussed. Results highlight the need to consider the appropriateness of a wind spectral model implemented in the strength design of FOWT structures.

Keywords: floating; wind; turbine; turbulence; intensity; strength; aerodynamic; coupling; nonlinear

1. Introduction

1.1 Introduction

Spectral models of dynamic wind are used to characterize the energy distribution of wind as a function of frequency. Fatigue and strength failures are the critical modes for wind turbine structures, and they are both highly sensitive to the characteristics of wind loading on the structure. In addition to hydrodynamic effects, aerodynamic impacts on the blades, tower, hull structure and mooring system are important. Thus, there is a strong need for the offshore wind industry to assess the characteristics of wind spectral models (associated with turbulence intensity) applied to the design of FOWTs, and their effects on responses of the blades, tower, platform and mooring system.

*Corresponding author, Ph.D., E-mail: Ikpoto.Udoh@atkinsglobal.com
[a] Ph.D., E-mail: Jun.Zou@atkinsglobal.com

http://www.techno-press.org/?journal=ose&subpage=7 ISSN: 2093-6702 (Print), 2093-677X (Online)

1.2 Previous research

Kaimal *et al.* (1972, 1976) developed what is now widely called the Kaimal spectrum with coherence, by studying the behavior of spectra and cospectra of turbulence in the surface layer using wind velocity and temperature, within the framework of similarity theory. Their work utilized experimental data obtained at specified elevations over a flat onshore site. A mathematical expression of the Kaimal spectrum is presented in Eq. (1).

The Froya turbulence wind model is derived based on wind turbulence data obtained at exposed sites along the western coast of Norway (Anderson and Lovseth 2006, 1992). Unlike the Kaimal model, the Froya spectrum is more suited for neutral atmospheric conditions (Anderson and Lovseth 2006), and may be inadequate in modeling sites that have significant atmospheric instability regimes. Eq. (2) is a mathematical expression of the Froya wind model. For offshore engineering applications, DNV-RP-C205 (DNV, 2007) recommends the application of Froya spectrum over Kaimal, stating that the low frequency energy is better estimated by the Froya spectrum.

Udoh and Zou (2016) and Udoh *et al.* (2016) studied the effect of wind turbulence on the responses of a TLP-type and a Semi-submersible-type floating wind turbine; system responses were assessed mainly via response spectra comparisons, and the Froya wind spectrum was not considered. Furthermore, wave loads were included in analysis, and attention was not given to the empirical distribution of extreme wind velocities and resulting responses.

1.3 Problem statement

Although Kaimal *et al*. (1972) show some correlation with data developed over water, this study considers the Kaimal spectrum as a good representation of land-based wind spectra, and the Froya model to generally represent offshore-based wind spectra. Ultimately, the analysis of offshore wind turbines will in many cases depend on numerical models of these spectrum types, rather than site-specific spectral models. Acknowledging the gaps between experimental observations and numerical modeling, it is critical to model and interpret wind effects correctly, to minimize the probability of erroneous or overly conservative designs.

Current industry interests indicate that the focus in wind energy development is intensely shifting from onshore to offshore sites. Methods and theories often used in onshore wind engineering analysis tend to be adapted as the norm in offshore wind analysis due to the lack of models and methods specifically developed for offshore wind applications. At a minimum, the design consequences of assuming onshore-related models for offshore wind analysis should be assessed and understood. A fundamental understanding of the impact of spectral formulations on offshore wind turbine responses is lacking in the industry, and should be developed, established and adopted by authorities. Such understanding is needed to address the following queries:

- To what extent does the choice of one spectral model affect the low frequency and high frequency responses of different components in a floating offshore wind turbine?
- What characteristics of wind spectra models drive differences in the response parameters, and how do these vary between models?
- What response interactions are most affected in the different frequency regimes, with changes to spectral parameters?

To address these queries, a quantitative and systematic assessment of coupled analysis responses is carried out. This paper focuses on extreme wind-induced effects for strength design; therefore, wave

and current loads are intentionally omitted. Wind spectra effects on fatigue design of floating wind turbines will be addressed in a sequel (Udoh and Zou, in preparation) to this paper.

2. Wind spectra models

2.1 Kaimal wind spectrum

The Kaimal wind spectrum is one of the most widely applied wind models in offshore wind projects. Its popularity in offshore wind analyses is perhaps enhanced by guidance provided by the International Electrotechnical Commission (IEC) for its application. As expressed in IEC 61400-1 (2005), a non-dimensional form of power spectral densities for the Kaimal model is

$$\frac{fS_k(f)}{\sigma^2{}_k} = \frac{4fL_k/V_{hub}}{(1+6fL_k/V_{hub})^{5/3}} \tag{1}$$

f is the frequency in Hertz

k denotes indices of the longitudinal (k=1), lateral (k=2) and vertical (k=3) components of wind velocities

S_k is the single-sided velocity component spectrum

σ_k is the velocity component standard deviation

L_k is the velocity component integral scale parameter

The associated turbulence spectral parameters (IEC 61400-1, 2005) applicable to the Kaimal model are presented in Table 1, in which Λ_u is the longitudinal turbulence scale parameter.

2.2 Froya wind spectrum

The Froya model as expressed in DNV-RP-C205 (DNV, 2007) is given in Eq. (2). The turbulence intensity associated with the Froya model is implicitly embedded in the formulation, such that it is a function of the wind speed used in analysis. The relationship between turbulence intensities of the longitudinal, lateral and vertical components of wind velocities applied in analysis with the Froya spectrum is the same as in the Kaimal spectrum: $\sigma_v = 0.8\sigma_u$ and $\sigma_w = 0.5\sigma_u$.

Table 1 Spectral Parameters of Kaimal Model

Parameter	**Velocity Component Index**		
	u	**v**	**w**
Standard Deviation, σ_K	σ_u	$0.8\sigma_u$	$0.5\sigma_u$
Integral Scale, L_K	$8.1\Lambda_u$	$2.7\Lambda_u$	$0.66\Lambda_u$

$$S(f) = 320\frac{\left(\frac{U_0}{10}\right)^2\left(\frac{z}{10}\right)^{0.45}}{\left(1+\tilde{f}^n\right)^{(5/3n)}} \quad (2)$$

$S(f)$ is the spectral or energy density function for frequency, f
U_0 is the 1-hr mean wind speed at 10 m elevation above the mean sea level
z is the height above the mean sea level in meters
$\tilde{f} = 172f\left(\frac{z}{10}\right)^{2/3}\left(\frac{U_0}{10}\right)^{-0.75}$ is a non-dimensional frequency
n = 0.468 is a non-dimensional coefficient

2.3 Spectral parameter considerations and wind modeling

Turbulence intensities applied in analysis with Kaimal wind spectrum are based on higher (A), medium (B) and lower (C) turbulence classes defined in IEC 61400-1 (2005), where the corresponding values are 16%, 14% and 12% respectively, for a mean wind speed of 50 m/s. For clarity, it is noteworthy that actual FOWT projects require the use of site-specific turbulence intensities as recommended by IEC 61400-3. However, it is common to encounter scenarios where site-specific turbulence data is unavailable, and values from IEC 61400-1 (intended for onshore applications) are resorted to. The Froya wind spectrum applied in analysis has a turbulence intensity of 10.4% for a mean wind speed of 50 m/s, and this prompted the consideration of an additional Kaimal spectrum with turbulence intensity of 10.4% for an equal-basis comparison (regarding turbulence intensities) with the Froya model. The IEC curves presented in IEC 61400-1 were traced as shown in Fig. 1, which also shows the Froya turbulence intensity curve as a function of wind speed. It should be noted that the turbulence intensity trend for the Froya model (Fig. 1) is consistent with site data and turbulence intensity models reported by Andersen and Lovseth (2006), for which turbulence intensity increases with reference wind speed. At typical operational wind speeds (~4 to 20 m/s), the disparity between IEC Class and Froya turbulence intensities is obvious and significant. Subsequent impacts on fatigue design are anticipated, but these results will be presented and discussed in a sequel paper as mentioned in Section 1. For wind speeds greater than 25 m/s, the turbulence intensity curves tend towards convergence, with much lower differences between IEC Class values and Froya. The differences observed between the Froya and IEC curves underscore the need for this study.

A comparison of longitudinal wind velocity spectral densities of Kaimal and Froya models (Fig. 2) shows that Froya has more energy in the low frequency region (0.01 Hz and lower), while Kaimal has more energy in other frequency regions. An empirical distribution function (defined in Eq. (3)) is used to represent the cumulative distribution of the extreme values. For each value of a variable x, the empirical cumulative distribution function $F_n(x)$, gives the fraction of the data less than or equal to x, for n observations in a dataset. The dynamic extreme tail distributions of horizontal wind velocities are compared in Fig. 3. Positive peaks of wind velocity timeseries form the upper tail, and negative peaks form the lower tail distributions. The left vertical axis and bottom horizontal axis of Fig. 3 relate to the upper tail distributions, while the right vertical axis and upper horizontal axis relate to the lower tail distributions. The lower tail distributions of Vy show that the extreme wind velocities from the Froya model exceed those of Kaimal-10.4% and Kaimal-C. For the Kaimal models, the dynamic extreme wind velocities trend consistently with turbulence intensities.

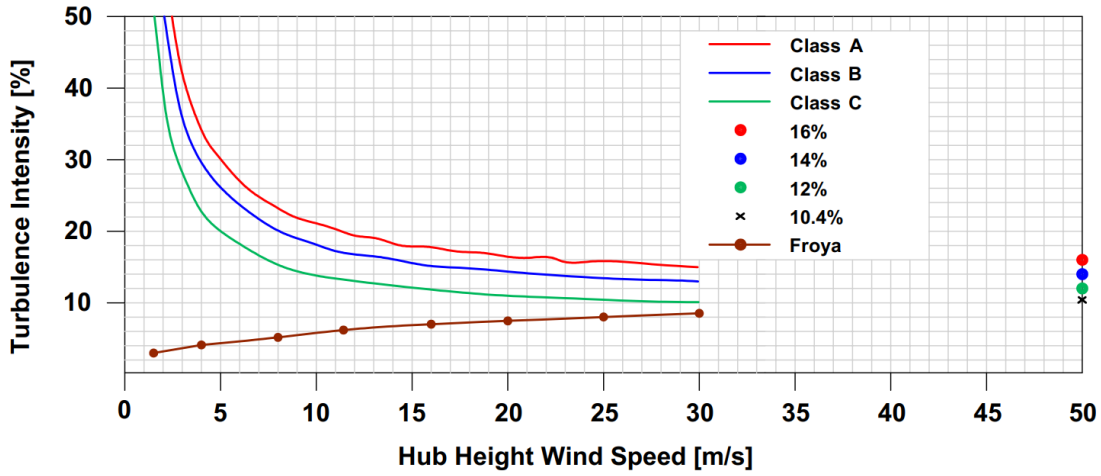

Fig. 1 Turbulence Intensity vs Hub Height Wind Speed

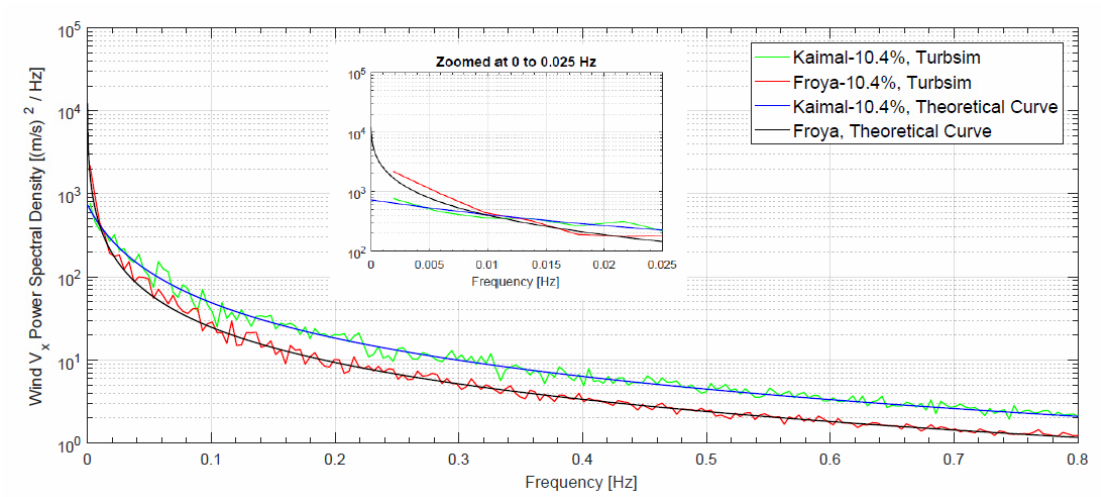

Fig. 2 Wind Spectra Comparisons – Turbsim vs Theoretical Curves, Mean Wind Speed = 50 m/s

The empirical distribution function is expressed with the Herd-Johnson estimator (Elsayed 2012) as

$$F_n(x) = \frac{1}{n+1}\sum_{i=1}^{n} \tau\{X_i \le x\} \tag{3}$$

where τ is an indicator function with conditions: $\tau\{X_i \le x\}$ is 1 if $X_i \le x$, and 0 otherwise.

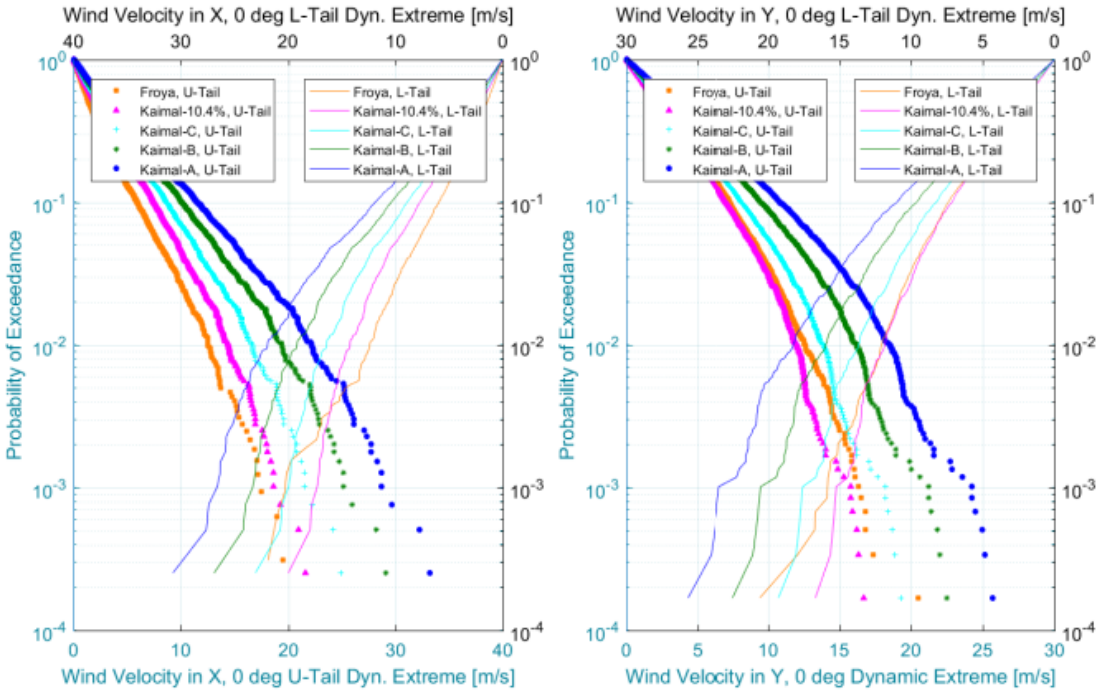

Fig. 3 Wind Velocity Extreme Distributions – Vx and Vy

3. Methods

3.1 System characteristics

The Paired-Column Semi-Submersible Floating Wind Foundation (P-C FWF) comprises of six columns (three inboard and three outboard). Inboard column dimensions and spacing can be efficiently optimized to support the tower and Rotor Nacelle Assembly (RNA) static and dynamic loads, while the outboard columns and spacing can be optimized for stability. Inner and outer column dimensions and spacing, as well as pontoon shape can be tuned to specific metocean criteria to yield the best performance of the wind turbine. Primary characteristics of the system are shown in Table 2, and the complete system is illustrated in Fig. 4. The 5 MW reference wind turbine developed by the National Renewable Energy Laboratory (NREL), USA, is implemented in analysis.

Natural periods of the platform, and modal periods of the tower and blades are shown in Table 3. The tower flexural properties are optimized to avoid resonance responses at the blade rotational and passing frequencies. In calculating the tower eigen periods, the RNA mass is included as a point mass at the towertop. Blade eigen modes are based on the distributed blade properties of the NREL 5 MW turbine (Jonkman *et al*. 2009).

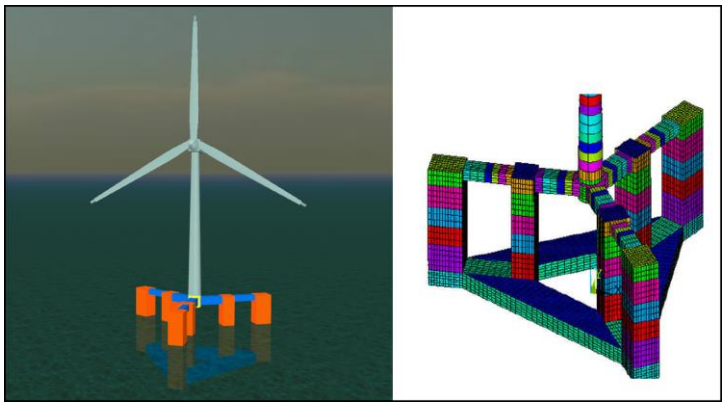

Fig. 4 PC-FWF Full View (left) and Mesh View of Hull (right)

Table 2 Key Figures of a 5 MW PC-FWF

Item	Unit	Value
Principal Dimensions		
Draft (In-place)[1]	[m]	16.0
Outer Column Size	[m]	9x7
Number of Outer Columns	[-]	3
Inner Column Size	[m]	6x7
Number of Inner Columns	[-]	3
Column Freeboard	[m]	15.0
Tower Top Diameter	[m]	3.87
Tower Base Diameter	[m]	6.50
Hub Diameter	[m]	3.0
Rotor Diameter	[m]	126.0
Hub Height (w.r.t. MLW)	[m]	90.0
Weight Data		
Displacement	[te]	10,650
RNA Mass	[mt]	350
Tower Mass	[mt]	425
Vertical Center of Gravity, VCG (w.r.t. Keel)[2]	[m]	11.72
Roll Radius of Gyration	[m]	28.79
Pitch Radius of Gyration	[m]	28.74
Yaw Radius of Gyration	[m]	24.83

1. Reference point of draft is platform keel.
2. VCG Reported includes free surface correction

Table 3 Natural / Eigen Periods of Platform, Tower and Blades

Platform Mode	Natural Period [sec]	Tower Mode	Eigen Period [sec]	Blade Mode	Eigen Period [sec]
Surge	69.5	Fore-Aft mode 1	2.23	Flapwise mode 1	1.48
Sway	68.0	Side-to-Side mode 1	2.27	Edgewise mode 1	0.90
Heave	20.0	Fore-Aft mode 2	0.37	Flapwise mode 2	0.52
Roll	24.5	Side-to-Side mode 2	0.46	Edgewise mode 2	0.25
Pitch	24.5	Twist mode 1	0.56		
Yaw	56.3				

3.2 Equations of dynamic analysis

Dynamics of a FOWT system can be represented by Newton's second law of motion, and these have been clearly detailed in Jonkman (2007). A simplified version of the linearized equations of motion (EOM) for a constrained FOWT platform is expressed in Eq. (4), which shows the components applicable to analysis performed in this research. By expressing the EOM in this form, the hydrodynamics are de-coupled from the body dynamics. Hydrodynamic components of Eq. (4) include the first order diffraction force $F_i^{D(1)}$, as well as added mass and radiation damping coefficients, a_{ij} and b_{ij}, respectively. The diffraction force is linearly proportional to incident wave amplitudes. Since wave and current loads are ignored in coupled analysis, the only active force driving the motions of the system is wind force, and $F_i^{D(1)}$ is ignored. The process used in deriving the EOMs used in coupled analysis, and expressions of the generalized active and inertia forces are discussed in Jonkman (2007). Bagbanci (2011) expresses Jonkman's (2007) generalized equations per system component – hub, nacelle, blades and tower, detailing the contributions of partial velocities and local accelerations to the forces acting on each. For the tower and blades, flexural properties (e.g., linear density and stiffness) contribute significantly to their dynamics and overall system responses.

$$M_{ij}\ddot{X}_j + K_{ij}X_j = F_i^{D(1)} - a_{ij}\ddot{X}_j - b_{ij}\dot{X} + F_i^{(wind + tower + nacelle + hub + mooring)} \quad (4)$$

In Eq. (4), M_{ij}, a_{ij}, b_{ij} and K_{ij} are the (i,j) components of the inertia mass, added mass, radiation damping and hydrostatic stiffness matrices, respectively. X , $\dot{X}$ and $\ddot{X}$ are displacement, velocity and acceleration of the floating platform and F_i is the net external force on the platform due to wind, mooring system, tower, nacelle, hub and blade dynamics.

3.3 Identification of tower – RNA coupled modes

Interactions between the tower and RNA are inevitable in floating offshore wind turbines. Frequencies at which these interactions occur must be identified, and any overlap in structural and global responses at such frequencies must be avoided. Such interactions have been reported to increase peak responses of the tower top significantly (Tong 2010). The extent to which the

coupling or interactions amplify system responses depend on specific seastate parameters and loading (i.e. operational or parked) conditions of the turbine.

Eigen frequencies of the tower–RNA responses are investigated by applying impulsive forces through 'hammer' tests. The platform is restrained from having significant translations or rotations using strings. The blades are feathered to a 90 deg pitch and the nacelle is yawed 90 deg. To isolate and identify effects of strings, the 'no load' condition with strings is simulated first, then impulsive forces are applied at the RNA (hub height) to excite the system in the global X, Y and Z directions (Xg, Yg and Zg, Fig. 6). The impulsive force (of 10,000 kN in Xg, and 5,000 kN in Yg and Zg) is applied after 100 secs (to allow sufficient decay of the initial dynamics of the system). The nacelle accelerations are recorded in each test.

In Fig. 5, time trains of "no load and string in X direction", "with impulsive load in X direction", "no load and string in Y direction" and "with impulsive load in Y direction" are displayed at the top panes (a, b, c, d) while the corresponding spectra are illustrated in the lower panes (e, f, g, h). In each spectrum plot, the blue line represents response spectrum in X direction and corresponding magnitudes are on the left vertical axis, while maroon lines represent the spectrum of Y-direction response with corresponding magnitudes on the right vertical axis. Responses in Z direction are not presented in Fig. 5.

Impulsive excitation of the RNA induces narrow-banded coupled responses of the RNA-tower assembly at distinct spectral peaks of 0.52, 0.54 and 0.56 Hz, as observed in the horizontal nacelle accelerations. When the RNA is excited horizontally, the dominant frequency of coupled nacelle accelerations in X and Y axes is 0.52 Hz. The response peaks at 0.54 and 0.56 Hz are found to be associated with transverse (when excitation is perpendicular to the rotor plane) and vertical accelerations (not shown) of the nacelle, and these two peaks are strongly coupled – although their overall spectral energies are an order of magnitude less than those observed at 0.52 Hz.

3.4 Coordinate systems and heading definitions

The origin of the global coordinate system Xg, Yg and Zg is located at the center of the tower in the horizontal plane, and at the mean water level (MWL) in the vertical plane, as shown in Fig. 6. Wind headings simulated in analysis are also shown in Fig. 6 – wind inflow at 0 deg is perpendicular to the rotor plane during which the nacelle and wind are aligned, while at 90 deg the wind is parallel to the rotor plane (i.e., perpendicular to the long side of the nacelle). Wind headings specified are with respect to the Xg axis, so that the wind heading is always equal to the nacelle-wind misalignment, and the nacelle is always aligned with the Xg axis as shown in Fig. 6. Local origins of the towerbase, nacelle and shaft coordinate systems used in analysis are shown in Fig. 7(a). Nacelle accelerations are calculated in the shaft coordinate system (x_s, y_s, z_s), and nacelle yaw is calculated in the nacelle coordinate system (x_n, y_n, z_n). The towerbase loads are calculated in the towerbase coordinate system (x_t, y_t, z_t).

Loads at the blade root consist of in-plane and out-of-plane shear forces and bending moments. Out-of-plane shear forces act along the $x_{b,i}$ axis shown in Fig. 7(b), while in-plane shear forces act along the $y_{b,i}$ axis. The out-of-plane and in-plane bending moments are caused by the out-of-plane and in-plane shear forces, respectively. It is noteworthy that the blade coordinate system pitches with the blades, so for a 90 deg blade pitch, the dominant shear for a 0 deg wind should be expected in the in-plane axis, and the dominant moment will be that caused by the in-plane shear force.

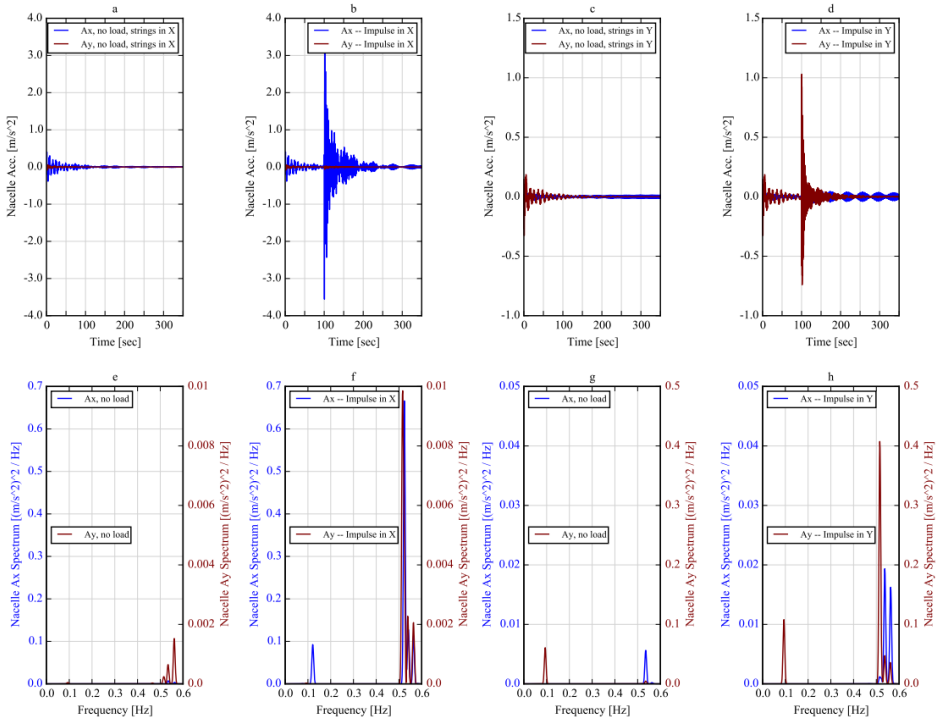

Fig. 5 RNA-Tower Coupling Frequencies

3.5 Load cases

Since strength design is the focus of this paper, only one extreme mean wind speed is considered, with a variation on the wind headings from 0 to 90 deg at 30 deg increments. Characteristics of the cases are summarized in Table 4. For all cases, the RNA is aligned with the Xg axis regardless of wind heading as shown in Fig. 6. The blade pitch angle is set to 90 deg for cases in 0, 30 and 60 deg wind headings. In the 90 deg wind heading cases, the blade pitch is set to 75 deg to avoid initial instabilities in the simulations. An idling state of the turbine is modeled in all cases, so the rotor experiences minor revolutions typically between 1 to 2 rpm.

Table 4 Load Case Characteristics

Hub Height Wind Speed	Platform Wind Speed at 10m above MWL	Wind Spectral Model	Turbulence Intensity	Wind Heading
[m/s]	[m/s]	[-]	[%]	[deg]
50.0	37.1	Froya	10.4	0, 30, 60, 90
		Kaimal-10.4	10.4	
		Kaimal-C	12.0	
		Kaimal-B	14.0	
		Kaimal-A	16.0	

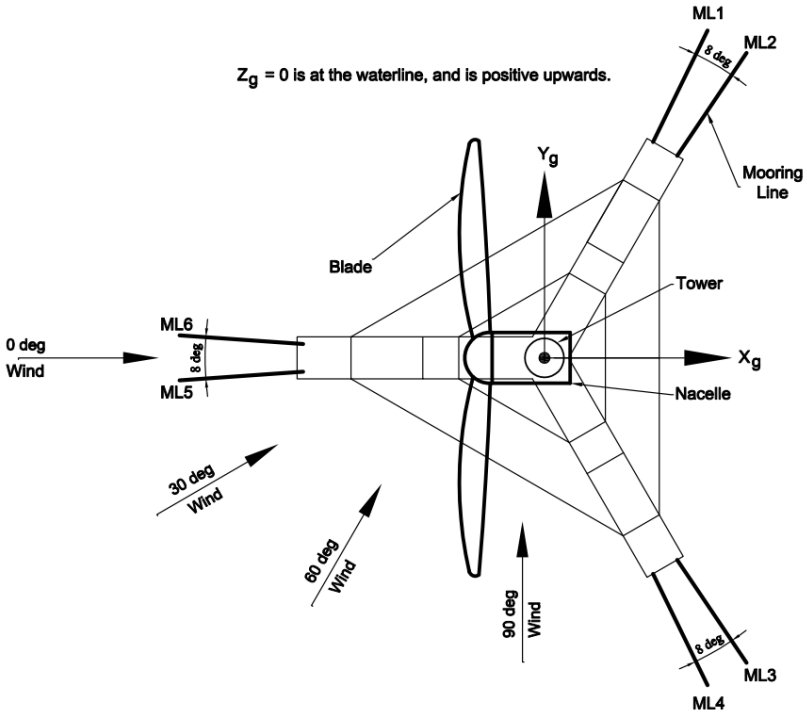

Fig. 6 Wind Headings, Global Coordinates and Mooring Line Identities

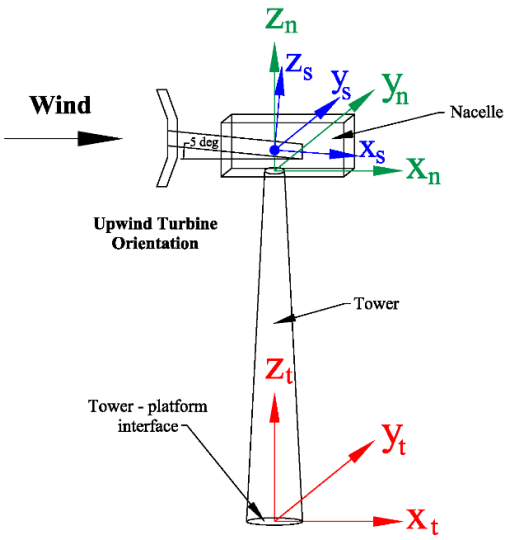

(a) Tower, Shaft and Nacelle Coordinate System in FAST

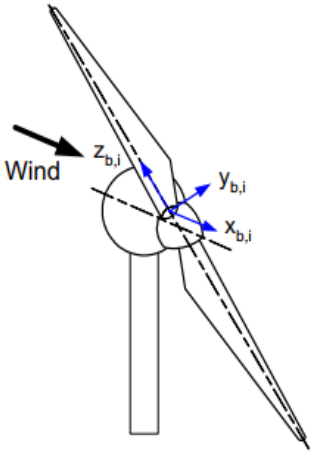

(b) Blade Coordinate System in FAST (Jonkman and Buhl 2005)

Fig. 7 RNA and Tower Coordinate Systems in FAST

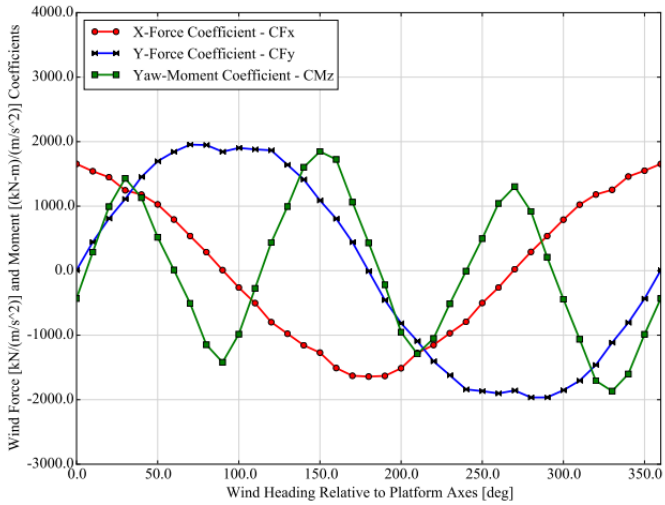

Fig. 8 Wind Force and Moment Coefficients

3.6 Coupled analysis and computer programs

Time domain coupled analysis is implemented to simulate the dynamic responses of the system. FAST (Jonkman and Buhl 2005) and OrcaFlex (Orcina Ltd.) are the two main programs used in the time domain simulations, with a dynamic link library called FASTLink (Orcina, Masciola *et al.* 2011) used to instantaneously exchange data between them. Aerodynamic, servo-dynamic and elastic effects on the tower and blades, and dynamics of the platform are calculated in FAST while dynamic responses of the mooring system are calculated in OrcaFlex. In each time-step, FAST combines the hydrodynamic loads received from OrcaFlex with aerodynamic loads calculated in FAST, to determine the instantaneous global motions, and dynamics of the tower, nacelle, blades and turbine components. Once that is completed, FAST transfers the resulting platform positions and velocities from the previous time-step to OrcaFlex for the next calculation of platform loads, and the process is repeated until the target simulation time is reached.

The tower eigen modes implemented in analysis are determined using BMODES (Bir 2007). Hydrodynamic added mass and radiation damping are calculated by WAMIT (WAMIT Inc. 2006). Line dynamics of the mooring system are obtained from OrcaFlex. For the 'idling' condition, wind forces and moments are estimated by WINDOS (MARIN, 2007) which is a program widely used in estimating wind loads on offshore structures.

Viscous damping is applied in coupled analysis as a percentage of critical damping in the system, in each respective mode of platform response. The percentages applied are derived from model test correlation analysis for similar floating structures, and are applied consistently for all types of wind spectra in analysis.

Turbsim (Jonkman and Kilcher 2012) is applied in generating full-field turbulent winds. The program has been widely implemented with common spectral models such as Kaimal and Froya (known in Turbsim as the API model) models. A grid size of 160 m x 300 m is used for all wind fields. It is noteworthy that in Turbsim, a target turbulence intensity can be specified and achieved for IEC models (such as Kaimal) using scaling parameters, but the program does not consider such

scaling for the Froya model. Therefore, in Turbsim, turbulence intensity for non-IEC models is largely dependent on, and sensitive to grid resolution.

In a previous project, a 5 MW NREL stock turbine was model-tested, and correlated WINDOS models for RNA and tower were established. The hull as illustrated in Fig. 4 is modeled in the correlated WINDOS model to generate resultant wind load coefficients which are presented in Fig. 8.

4. Result observations

Although four headings are simulated in analysis, graphical results are mostly shown for 0 deg wind heading for brevity. Statistics of selected responses for all wind headings simulated are discussed in Section 4.9. Empirical distribution functions for each response parameter are used to assess the influence of each wind spectra type on the extreme responses. The probabilities of exceedance are not the focus for comparing the responses (since they are quite close at the tails), rather the dynamic extreme values are assessed for comparisons. Bar charts of the statistics are reported for each response parameter. In some cases, root-mean-square (RMS) and dynamic extreme results are reported as ratios, where the response from the Froya wind model is used to normalize all responses such that the Froya response ratio is always 1.0. However, bar charts of the total and extreme factor values (calculated as the ratio of dynamic extreme to RMS) show the actual values and not ratios, to provide a delineation of the relative magnitudes of the different response components. Magnitudes of the extreme factors offer an understanding of the linearity (or nonlinearity) of the responses.

4.1 Nacelle accelerations

Fig. 9 shows extreme distributions of translational accelerations of the nacelle in 0 deg wind heading. Translational accelerations of the nacelle indicate very little variation per spectra type in the dominant component, but show clear variations in the weaker component of response. In 0 deg wind, nacelle Ax is the dominant translational acceleration, and its spectra (not shown) as well as upper and lower tail empirical distributions (Fig. 9) of all considered wind spectral models are very similar in magnitude. Magnitudes of nacelle Ay responses are lower than Ax, and responses of Kaimal model generally trend with turbulence intensity. The dynamic extreme (lower tail) of the Froya nacelle Ax response exceeds that of the Kaimal-10.4 and Kaimal-A models, though the difference is practically insignificant. Lower tail distributions of nacelle Ax exceed upper tail distributions by around 10%, indicating a mildly non-linear response. Low frequency and high frequency (at 0.52 Hz) accelerations are observed in nacelle Ax, with more energy in the low frequency region.

Magnitudes of rotational accelerations (not shown) of the nacelle in 0 deg are consistent with their corresponding translational accelerations. With Ax being the dominant translational response, pitch acceleration (which is associated with Ax) is higher than roll accelerations. Dynamic extremes of pitch accelerations from the different wind spectra differ by less than 10%, and their spectral densities show no significant differences in low and high frequency regions. Roll accelerations however indicate a strong variation (over 40% difference between Kaimal-10.4% and Kaimal-A) in dynamic extremes and spectral densities for the Kaimal models, which are quite consistent with turbulence intensities of the wind spectra.

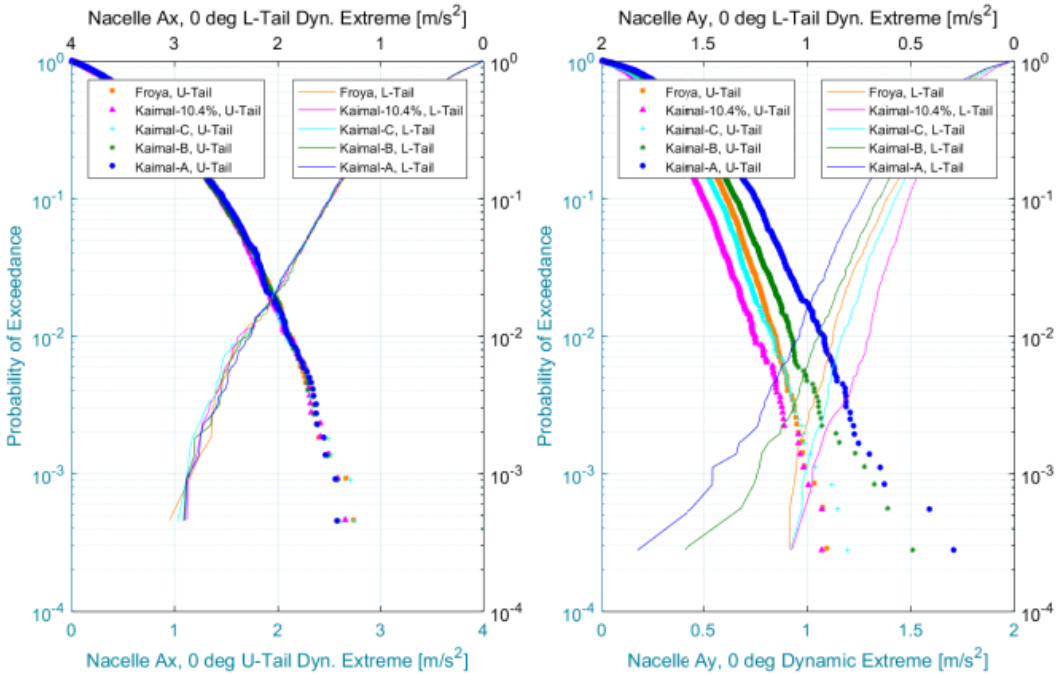

Fig. 9 Nacelle Translational Accelerations in 0 deg Wind

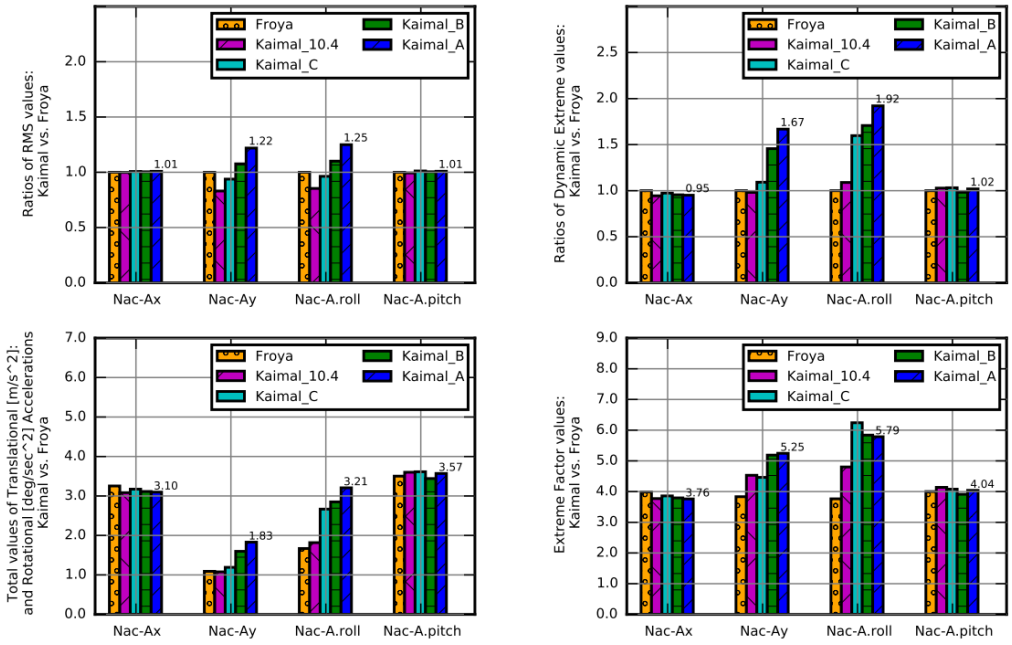

Fig. 10 Statistics of Nacelle Accelerations in 0 deg Wind

Statistics of translational nacelle accelerations are compared for 0 deg wind heading in Fig. 10. Comparisons show that the extreme factors are not strictly correlated with turbulence intensity, and that the weaker responses in this case (nacelle Ay and A-roll) are mostly non-linear, with extreme factors of Kaimal-A up to 5.3 and 5.8 for Ay and A-roll, respectively. Ratios of RMS values show consistency with turbulence intensity among the Kaimal models, for nacelle Ay and A-roll accelerations, and practically no variation in Ax and A-pitch accelerations. RMS ratios also indicate that the Froya model has more spectral energy in nacelle Ay and A-roll, compared to Kaimal-10.4% and Kaimal-C. Empirical distributions of the extreme wind velocities (Fig. 3) in Xg and Yg directions indicate that the Froya upper and lower tail extremes of Vy, and the lower tail extreme of Vx exceed those of Kaimal-10.4%, which has the same turbulence intensity as the Froya wind field. Essentially, the tail distribution of the Froya model differs from that of Kaimal models. Interestingly, not only do the Froya Ax total nacelle accelerations exceed those of Kaimal-10.4%, they exceed those of all other Kaimal spectra with higher turbulence intensities – but the differences are marginal.

4.2 Blade root loads

In-plane shear forces and bending moments are the dominant loads at the blade root. Only the 0 deg blade root results are discussed here, because the timeseries data for blade root responses in 30, 60 and 90 deg are quite erratic when the blades are loaded from oblique directions resulting in significant changes in the mean loads. For such data, the empirical distributions functions are discontinuous, making the determination of dynamic extremes inconsistent – relative to smooth trends as shown for 0 deg wind in Fig. 11.

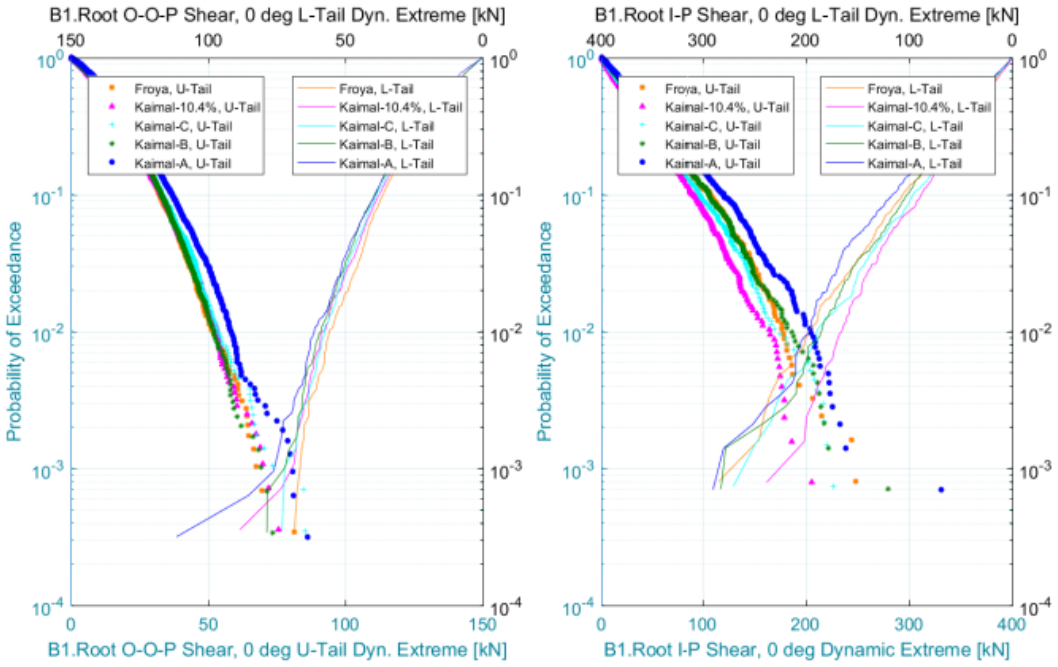

Fig. 11 Blade Root Shear Forces in 0 deg Wind

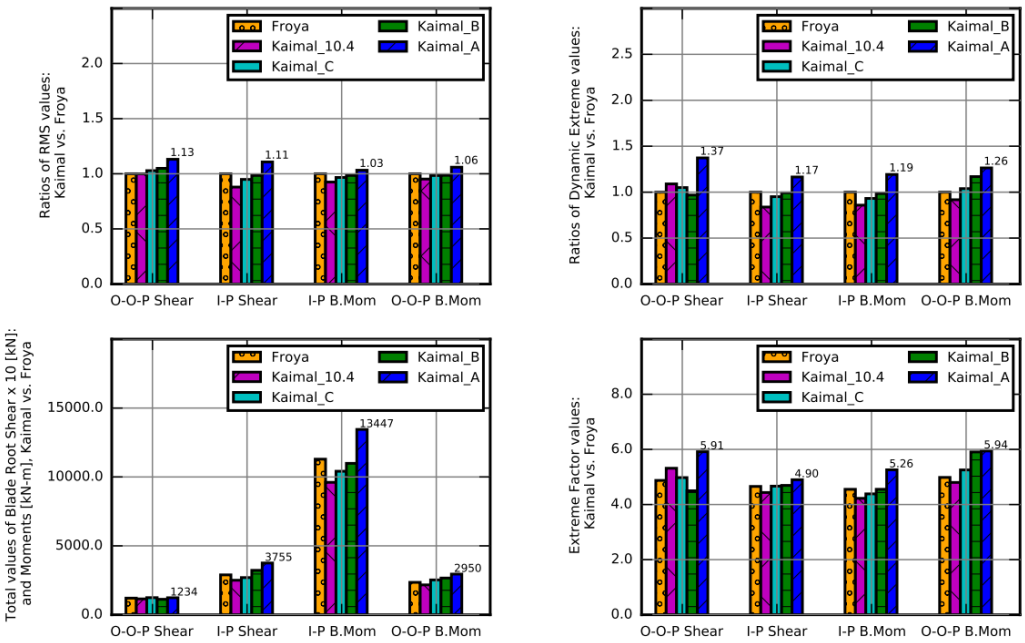

Fig. 12 Statistics of Blade Root Loads in 0 deg Wind

Empirical distribution plots of the blade root loads are given in Fig. 11. Low frequency responses (spectral plots not shown) are dominant in the in-plane shear and moments, while relatively insignificant spectral energy can be seen in the out-of-plane loads. The empirical distribution plots indicate that the extreme in-plane shear and moments for the Kaimal model increase with turbulence intensity, while the Froya model generally has dynamic extreme values that exceed Kaimal 10.4% and Kaimal-C spectra. The magnitudes of out-of-plane loads is about 20% of their corresponding in-plane loads, with extreme values of the lower tails consistent with the empirical distributions of the wind speeds. The upper tail extremes of the out-of-plane shear and moments are not consistent with the turbulence intensity trends.

Bar charts comparing the statistics of blade root loads for different wind spectra are reported in Fig. 12. It should be noted that the total shear force values plotted are intentionally multiplied by a factor of 10 to increase visibility of the trends on the plots. The total values show modest variations in the out-of-plane loads, but indicate a strong variation in in-plane moments for the different spectra. Total in-plane moment from the Froya model exceeds Kaimal extremes, except Kaimal-A. The dynamic extreme of the Kaimal-A in-plane loads exceed Froya extremes by almost 20%, but the Froya dynamic extreme exceeds Kaimal-10.4% by close to 30%. The RMS values increase with turbulence intensity for the Kaimal models, as was observed in the nacelle accelerations. Extreme factors of the blade root loads range from 4.9 to 5.9, indicating a mildly-nonlinear characteristic of the blade root loads.

4.3 Towertop motions

Like nacelle accelerations, the fore-aft displacement and pitch rotation of the towertop are the dominant components of towertop response in 0 deg wind. In this heading, observations in spectra (not shown) indicate predominantly low frequency energy, with some high frequency contribution at 0.52 Hz for fore-aft displacement and towertop pitch. Dynamic extreme distributions of the fore-aft displacement show little or no variation with spectra for 0 deg wind, in both upper and lower tails; it is however seen that the fore-aft displacement and pitch rotation of the Froya model exceeds those of Kaimal-A, Kaimal-B and Kaimal-10.4%. Therefore, the dynamic extremes of the dominant towertop motions in 0 deg do not trend with turbulence intensity. Clearer trends consistent with increase in turbulence intensity are seen in the side-to-side displacement and roll rotations, which are the weaker response components of displacement and rotations, respectively.

Comparisons of statistics (Fig. 13) show no significant changes in RMS and dynamic extreme values with different spectra in fore-aft displacements and pitch motions of the towertop, in 0 deg wind. Side-to-side and roll motion RMS and dynamic extremes vary more significantly with wind spectrum type; the differences are about 20% in RMS and 37% in dynamic extreme between Froya and Kaimal-A. Extreme factors of fore-aft displacements and pitch towertop rotations are about 3.8, indicating a linear characteristic of the responses. The side-to-side and roll motions have higher extreme factors (4.0 – 4.6), and do not follow a trend – the magnitudes suggest a mildly non-linear characteristic of the weaker responses, although their practical significance may not be high considering that the actual values of towertop side-to-side and roll motions are generally quite low.

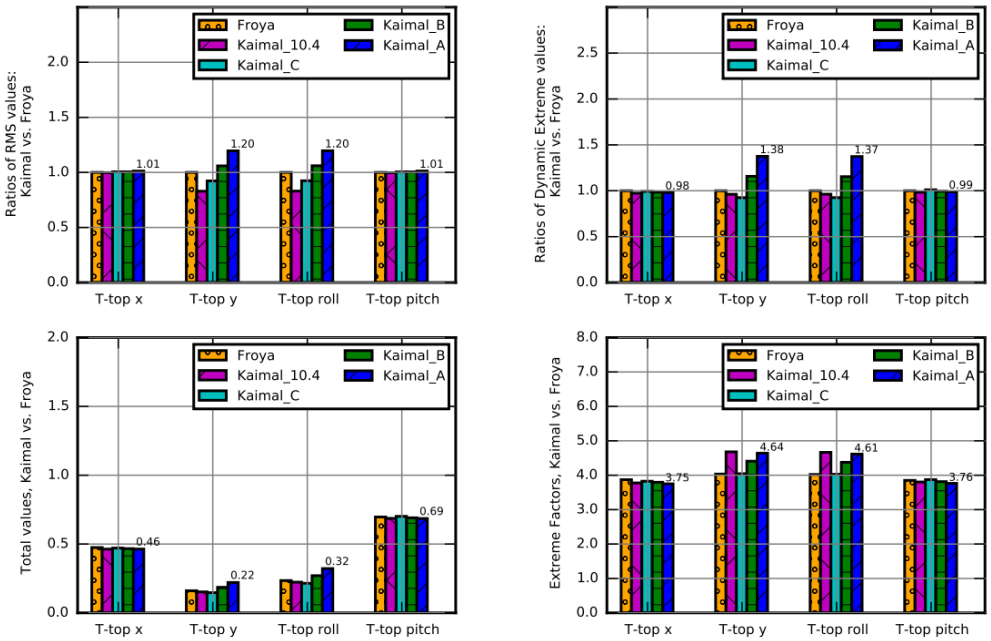

Fig. 13 Statistics of Towertop Displacements in 0 deg Wind

4.4 Towerbase loads

The towerbase or tower-platform interface is one of the most critical loading sections of a floating offshore wind turbine. Shear forces about the towerbase section are shown in Fig. 14 for 0 deg wind condition. RMS and dynamic extreme trends of the forces and moments are generally like those reported in earlier sections, regarding dominant and weaker response components per wind heading. In 0 deg wind, dynamic extreme peaks of towerbase Fx and My (which are associated) have little or no variation with different wind spectra. Upper and lower tails of the extreme distributions are very similar in magnitude for towerbase Fx and Fy. For the Kaimal wind spectra, a clear trend is seen in dynamic extremes of towerbase Fy with respect to turbulence intensity. In 0 deg wind heading, the Froya model produces a towerbase Fy force of ~600 kN, exceeding values of Kaimal-B, Kaimal-C and Kaimal-10.4% (~450 kN) which have higher wind turbulence intensities. Spectral energies of towerbase Fx and My in 0 deg show minor variations with the different spectra, but variations among the Kaimal models trend with wind turbulence intensity.

Fig. 15 shows the comparison of statistics for the towerbase loads in 0 deg. The trends mentioned earlier are reflected in the RMS and dynamic extreme ratios shown. It is noteworthy that the total towerbase forces shown in Fig. 15 are intentionally scaled up by a factor of 10 to aid the visibility of the trends on the bar chart. For the Fy and Mx loads in 60 deg, dynamic extremes of the Froya model exceed Kaimal-A loads by 10%; this is not trivial, since the magnitudes of the Fy and Mx loads in 60 deg are higher than Fx and My loads.

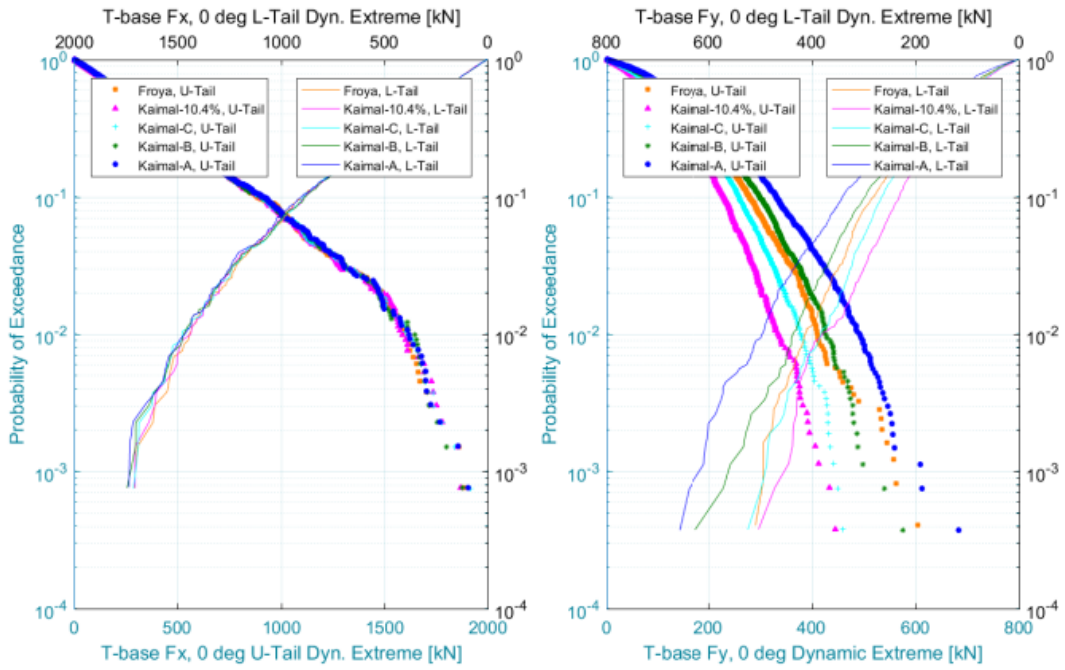

Fig. 14 Towerbase Shear Forces in 0 deg Wind

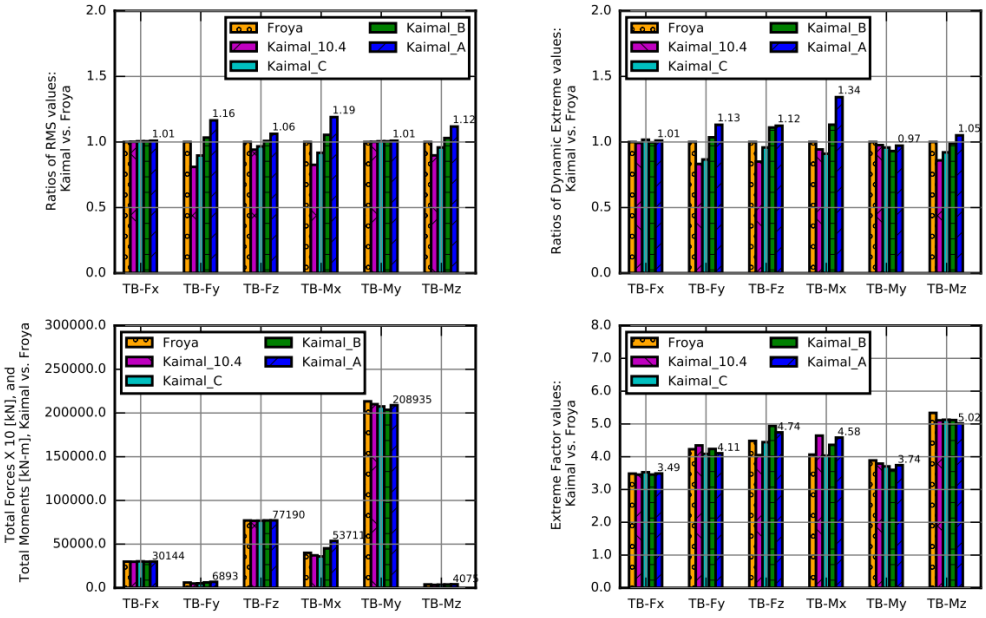

Fig. 15 Statistics of Towerbase Forces and Moments in 0 deg Wind

The comparisons imply that the resultant loads can be significantly affected by changes in wind spectra. Extreme factors of towerbase loads are generally higher in 60 deg wind heading than in 0 deg wind. Relatively higher non-linearity is observed in towerbase vertical force (Fz), and moment about the vertical axis (Mz). Changes in extreme factors with wind spectrum is most significant in towerbase Fy, Mx, Fz and Mz, and these changes do not follow a consistent trend.

4.5 Platform motions

Important response modes of the platform that are assessed in this paper are roll and pitch. The rotations (roll / pitch) of the platform are critical to wind turbine loads than translational motions, because of the significant moment arm which is essentially the hub height of the system relative to the waterline. Translational motions are however still compared to understand the influence of different wind spectra on the responses.

Pitch motions of the platform are the dominant rotations in 0 deg wind (Fig. 16), and the variations in dynamic extreme and spectra with the different wind spectra, are negligible. Platform roll, being the weaker response in 0 deg, shows significant variations with wind spectra (as indicated by the RMS values in Fig. 17), and for the Kaimal models the upper tail distribution is consistent with turbulence intensity.

4.6 Platform accelerations

Accelerations at the center of gravity of the platform and their statistics are shown in Fig. 18. The translational acceleration trends are very similar to those reported for other response

parameters – little or no variation in dynamic extremes and spectra of the dominant response in 0 deg (in this case, platform Ax), and clearer trends (upper tails trend with turbulence intensity) in the weaker response (platform Ay). The translational accelerations are low frequency dominant, with some variation in spectral density magnitudes with different wind spectra.

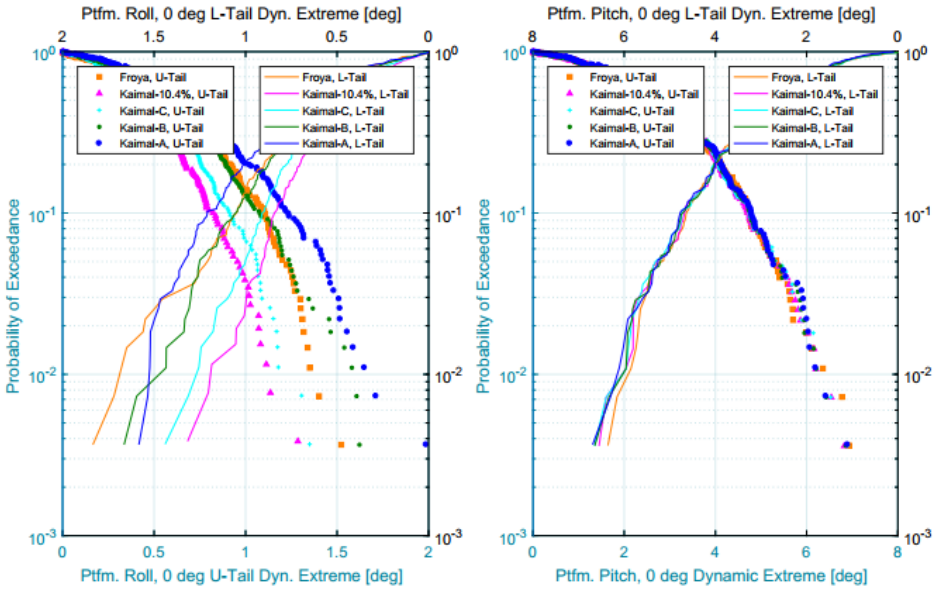

Fig. 16 Platform Roll and Pitch in 0 deg Wind

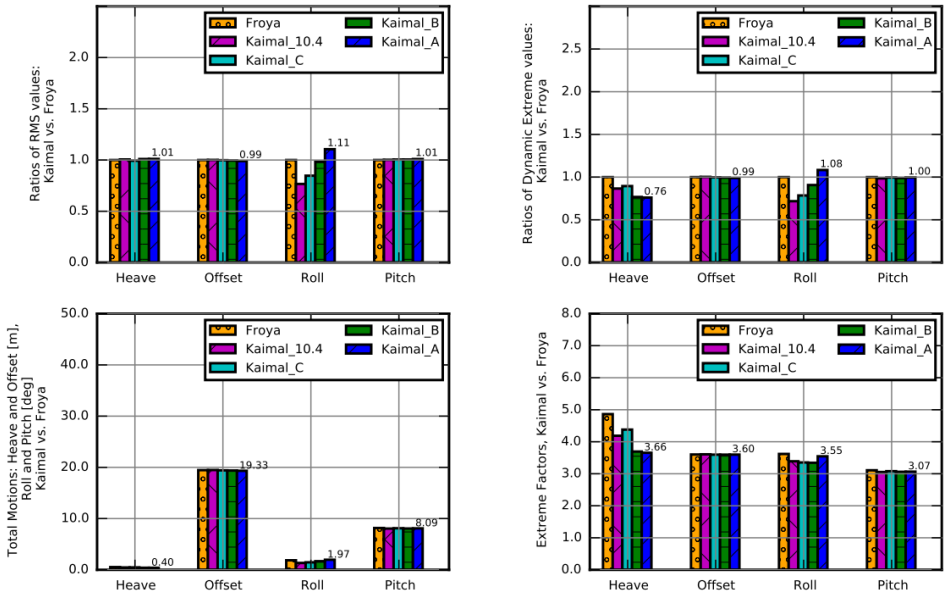

Fig. 17 Statistics of Platform Motions in 0 deg Wind

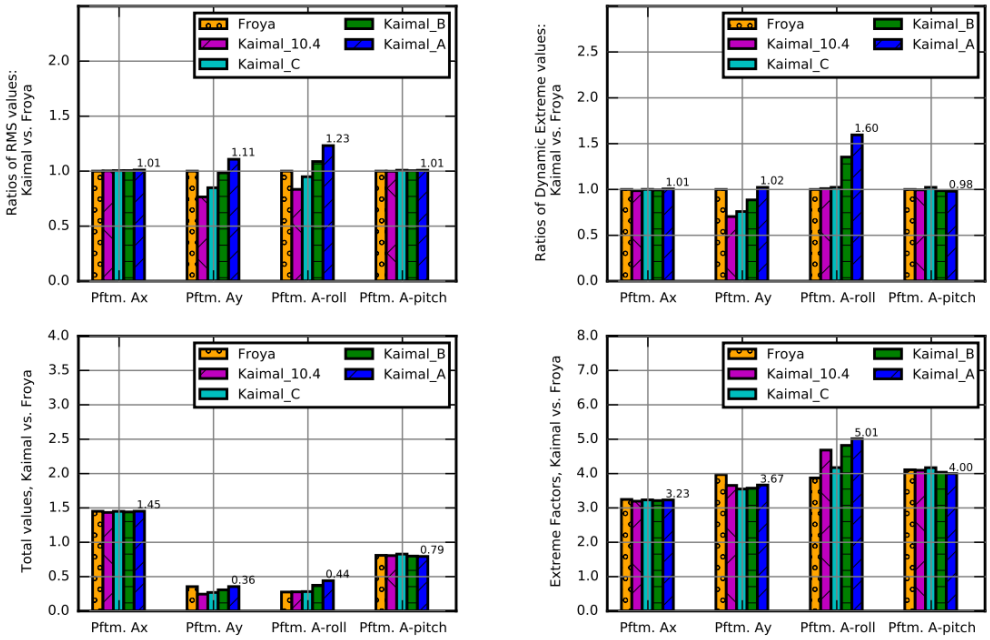

Fig. 18 Statistics of Platform Accelerations in 0 deg Wind

Rotational accelerations of the platform CG have both low and high frequency components, and interestingly, the variations in energy spectra (though with relatively small differences) are more existent in the high frequency regions, while the low frequency roll and pitch accelerations practically do not change with different wind spectra.

Statistics of platform accelerations are compared in Fig. 18 for 0 deg wind. The bar charts show that only the non-dominant acceleration components have significant percentage differences in RMS, dynamic extreme, total accelerations and extreme factors, with respect to wind spectra. Extreme factors of platform roll accelerations are higher than those of other components, but have modest practical significance given the actual magnitude of the roll acceleration responses in 0 deg,

4.7 Mooring line tensions

Extreme tensions of mooring lines govern their strength design, therefore, understanding the impact of wind spectra characteristics is important. Mooring line tensions are presented in Fig. 19. In 0 deg wind, the upwind mooring lines ML 5 and ML6 (see mooring line numbering in Fig. 6) are the most loaded lines, and tensions in these lines do not change with the different wind spectra, as all spectral densities and dynamic extremes essentially converge to almost the same values. Higher magnitudes of dynamic extreme tensions in ML5 and ML6 are skewed towards the upper tail distributions, indicating some non-linearity in the tensions – consistent with the extreme factors for ML5 and ML6 which are approximately 4.20 (Fig. 20). ML3 and ML4 are tangential lines relative to the axis of loading (i.e., in 0 deg wind); their tensions show more variation with

different wind spectra, in both RMS and dynamic extremes (Fig. 19), where the lower tails of dynamic extreme tensions for Kaimal models trend with turbulence intensity, and the upper tails do not follow a consistent trend.

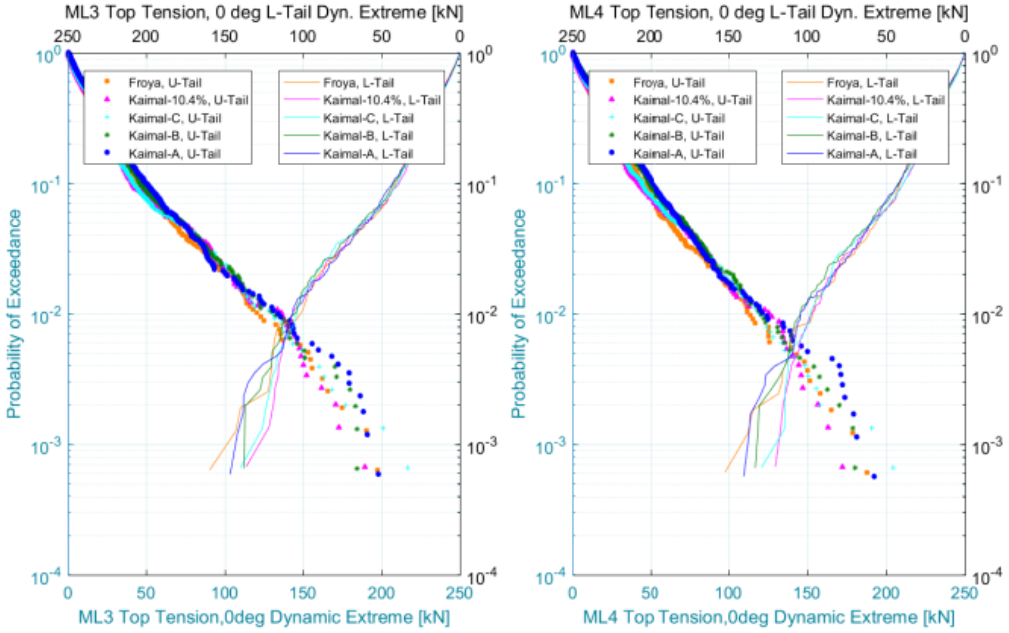

Fig. 19 ML3 and ML4 Tensions in 0 deg Wind

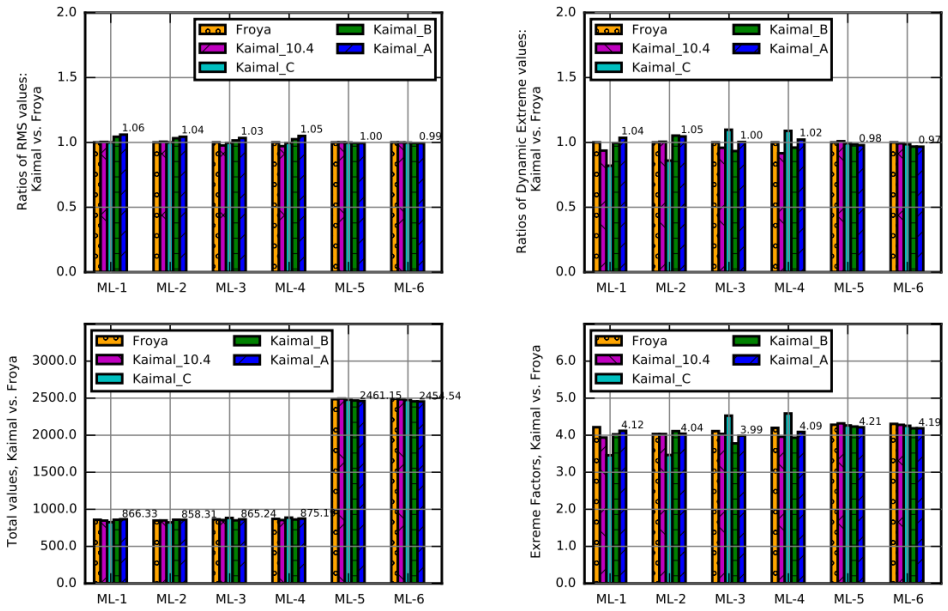

Fig. 20 Statistics of Mooring Line Tensions in 0 deg Wind

Statistics of mooring line tensions show that the less loaded lines in 0 deg (Fig. 20) have the most variations with wind spectra, and for these lines RMS values for the Kaimal models trend with turbulence intensity. Extreme factors for all lines range from 4.0 to 4.2, indicating a generally weak non-linear characteristic of the tensions. In the total tensions, less variation is seen regarding wind spectra because the mean tensions are high relative to dynamic tensions.

5. Discussions

5.1 Coupled response interactions

Coupled interactions between the nacelle and tower were presented in Section 3.3 and the lowest eigenfrequency is at 0.52 Hz. Figs. 21 and 22 are spectra of nacelle rotational accelerations and platform rotational accelerations in 60 deg wind, respectively. These results are selected for discussion because of the relative magnitudes of low and high frequency components in their energy spectra.

Nacelle roll and pitch accelerations (Fig. 21) are high-frequency dominant, and some slight variations in spectral density is observed in around 0.52 Hz. This dominance of high-frequency over low frequency accelerations is not found in the towertop motions in 60 deg wind, although the towertop motions contain significant high frequency energy. The high-frequency interactions at the nacelle are transferred to the platform (Fig. 22), as the platform rotational accelerations contain some energy at 0.52 Hz.

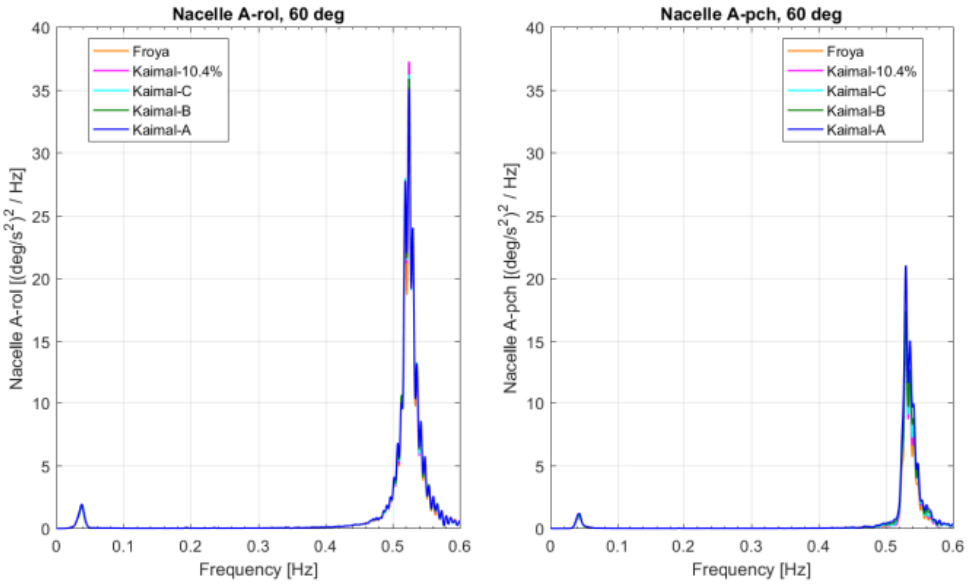

Fig. 21 Nacelle Rotational Accelerations in 60 deg Wind

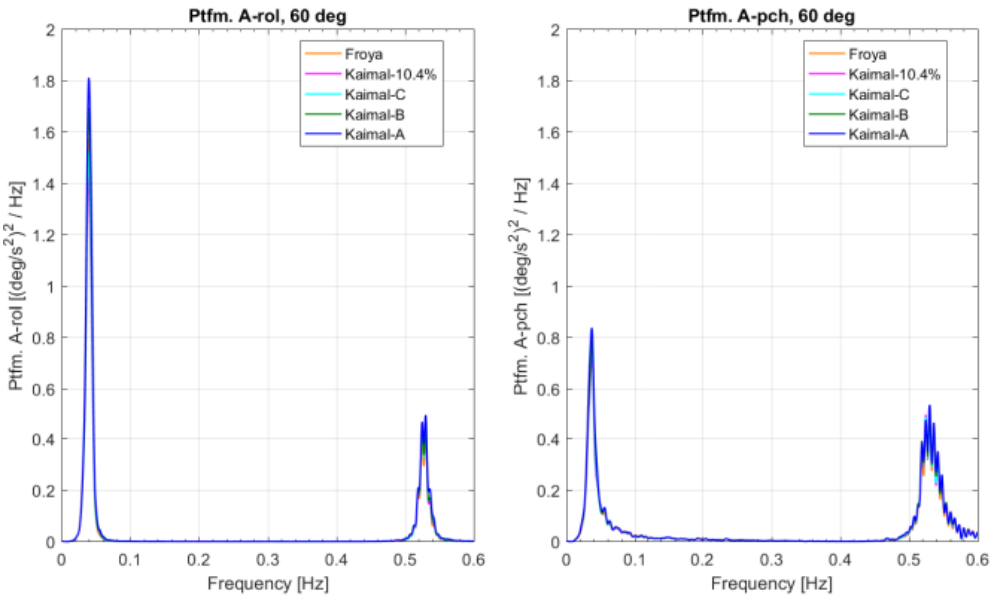

Fig. 22 Platform Rotational Acceleration in 60 deg Wind

Comparing the magnitudes of nacelle roll and platform roll acceleration spectra, the high frequency (at 0.52 Hz) energy at the nacelle is at least 35 deg/s^2 / Hz, while that of the platform is approximately 0.5 deg/s^2 / Hz. The low frequency energy acceleration at the nacelle slightly exceeds that at the platform. At the nacelle, the low frequency spectral energy is less than 7% of the high frequency energy (for roll and pitch), but at the platform, the low frequency energy is about 27% and 60% of the roll and pitch high frequency accelerations, respectively. The significant dominance of high frequency accelerations at the nacelle, indicates the importance of modeling the tower-nacelle interactions accurately. Reduced high frequency content of platform accelerations indicate that such interactions are damped to a significant extent as they are transferred through the tower structure to the platform.

Of all results, rotational accelerations of the nacelle and platform have the most significant high frequency energy. Not only are the high frequency responses significant, the variations with wind spectral models are higher at 0.52 Hz than in the low frequency region. It should be noted that the high-frequency responses are not seen in translational accelerations of the platform, even though the translational accelerations of the nacelle contain significant high frequency energy. Thus, the primary mode of transfer of high frequency tower-nacelle interactions to the platform, is via rotations of the nacelle or RNA.

It is worth pointing out that the tower should not be modeled as a rigid body together with the platform hull. Modeling the flexure of the tower enables the capturing of high frequency response phenomena, and it is important to capture such effects to fully represent the behavior of the real tower-nacelle system in the installed condition.

5.2 Response statistics relative to wind heading

Due to brevity, two important components: nacelle accelerations and towerbase loads, are selected for comparison of statistics relative to wind heading. Figs. 23 and 24 present statistics of translational and rotational accelerations of the nacelle, respectively, while statistics of towerbase shear forces and bending moment are presented in Figs. 25 and 26, respectively. In these figures, the horizontal axis labels such as '0x', and '90y' indicate the heading and component axis of the response – where '0x' means x-component of response in 0 deg wind, and '90y' means y-component of response in 90 deg wind. In Fig. 24, '0r' and '30r' represent nacelle roll accelerations in 0 deg and 30 deg, respectively, while '0p' and '30p' represent nacelle pitch accelerations in 0 deg and 30 deg, respectively, and so on. 'Kaimal D' represents Kaimal-10.4% spectrum.

RMS comparisons of nacelle translational accelerations indicate highest magnitudes in 0 deg for Ax component, and 90 deg for Ay component – consistent with wind coefficients. The weaker headings (relative to response component) have more variation in RMS, with different wind spectra.

So, more variation is seen in 90 deg wind heading (compared to other headings) for Ax and A-pitch acceleration, and more variation is seen in 0 deg for Ay and A-roll. Variation of RMS with different spectra is less in the oblique headings (30 and 60 deg), and the trends are consistent with turbulence intensity for translational and rotational components of nacelle acceleration. The decrease or increase in RMS of Ax, Ay, A-roll and A-pitch with wind heading is seen to be non-linear; for instance, there is a more significant drop between 0 and 30 deg of Ay compared to other adjacent headings. RMS of nacelle pitch accelerations correlate with Ax accelerations, while roll accelerations correlate with Ay – these are reflected in the RMS trends of Figs. 24 and 25.

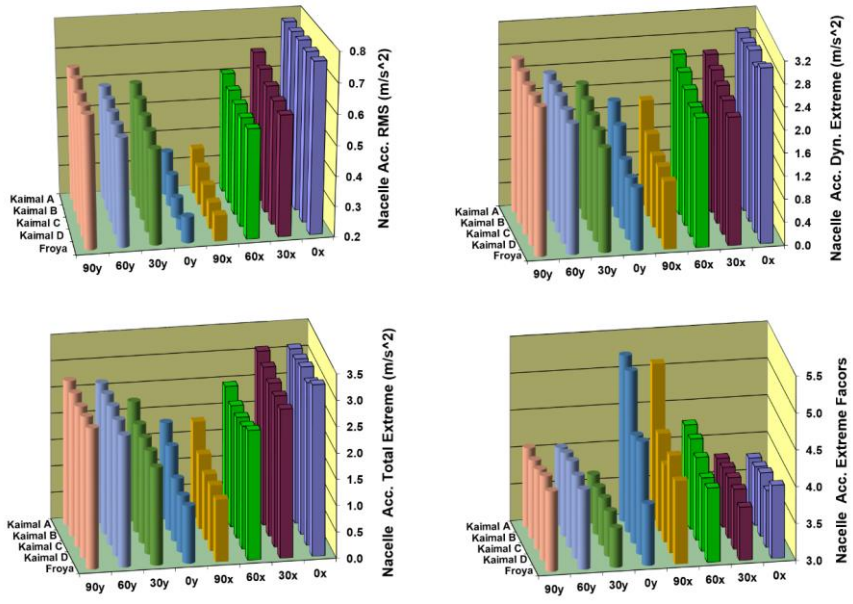

Fig. 23 Statistics of Nacelle Translational Accelerations – 0, 30, 60 and 90 deg Wind

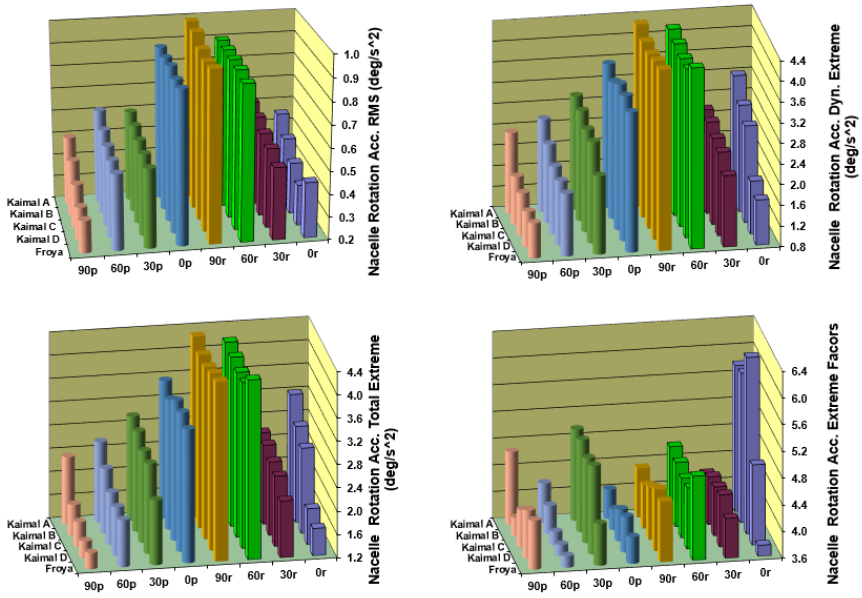

Fig. 24 Statistics of Nacelle Rotational Accelerations – 0, 30, 60 and 90 deg Wind

Dynamic extremes of translational and rotational nacelle accelerations follow very similar trends as the RMS in terms of relative magnitudes per wind heading, and increase in variation per spectra type at the weaker headings (with respect to response component). The total translational and rotational accelerations also follow similar trends described prior, mainly because the mean accelerations are practically negligible, hence cannot alter the trends significantly.

Extreme factors of nacelle accelerations do not trend with turbulence intensity. It is found in 0 deg and 90 deg wind headings of translational accelerations, that Kaimal models (especially Kaimal-A) have more non-linear extreme factors in the weaker response components. Variations in extreme factors of nacelle translational accelerations are much less in 30 and 60 deg wind headings, and the values range from 3.7 in 30 deg (linear or Gaussian characteristic) to 4.6 in 60 deg (mildly non-linear characteristic). Although the trends of dynamic extreme and RMS are consistent between translational and rotational nacelle accelerations, the extreme factors result from the actual magnitudes for each case. Extreme factors of nacelle rotational accelerations do not trend consistently with wind heading or spectra, and go as high as 6.0 for roll acceleration in 0 deg wind. High non-linearity of accelerations is a characteristic that can impact negatively on the strength of the nacelle. Since the relatively high extreme factors occur at weaker responses or headings, the impact is likely to be significant on the strength of the nacelle if the magnitude of weaker response's dynamic extreme is quite comparable to that of the stronger component or heading.

Towerbase shear forces (Fig. 25) in 0 deg also indicate stronger variations in RMS of the weaker responses (Fy in 0 deg), however, in 90 deg, the weaker response component (Fx) shows no significant variation with the different wind spectra types. RMS values of Fx shear forces vary almost linearly with heading, while the relationship between the Fy RMS values and wind heading

is not linear at all – there is a significant difference between the 0 and 30 deg magnitudes, compared to the difference between 30 and 60 deg. Dynamic extremes of Fx trend with turbulence intensity for all headings, while Fy shear force does not have such consistency – trends of the Kaimal models increase with turbulence intensity for 0 and 30 deg, but are inconsistent for 60 and 90 deg. In 60 deg wind, Fy shear force which is the dominant shear has a reversed trend with turbulence intensity for Kaimal-D, Kaimal-C and Kaimal-B, although the percentage differences between the Fy shear values are small. This is a unique behavior, showing that with increased turbulence intensity, the loading and interactions in the system in 60 deg wind results in reduced Fy shear for the three models mentioned. The total shear forces follow a very similar trend to that of dynamic extremes, with the exception that total Fx shear in 30 deg dominates the shear forces, implying that the mean Fx force in 30 deg wind exceeds the 0 deg value.

Statistics of bending moments RMS, dynamic extreme and total values are very similar, and are consistent with the dynamic extreme shear force trends, as expected. Where the Fx shear force dominates, the associated My moment dominates. Variations with respect to wind spectra seen in the shear forces reflect in the moments. Extreme factors of the shear forces and bending moments vary significantly with heading and spectra, with no clear trend on either heading on spectrum type.

For both shear forces and bending moments, Kaimal models in 90 deg wind heading produce the highest extreme factors (up to 4.7 in My of 90 deg wind), and their trends do not correlate with turbulence intensity.

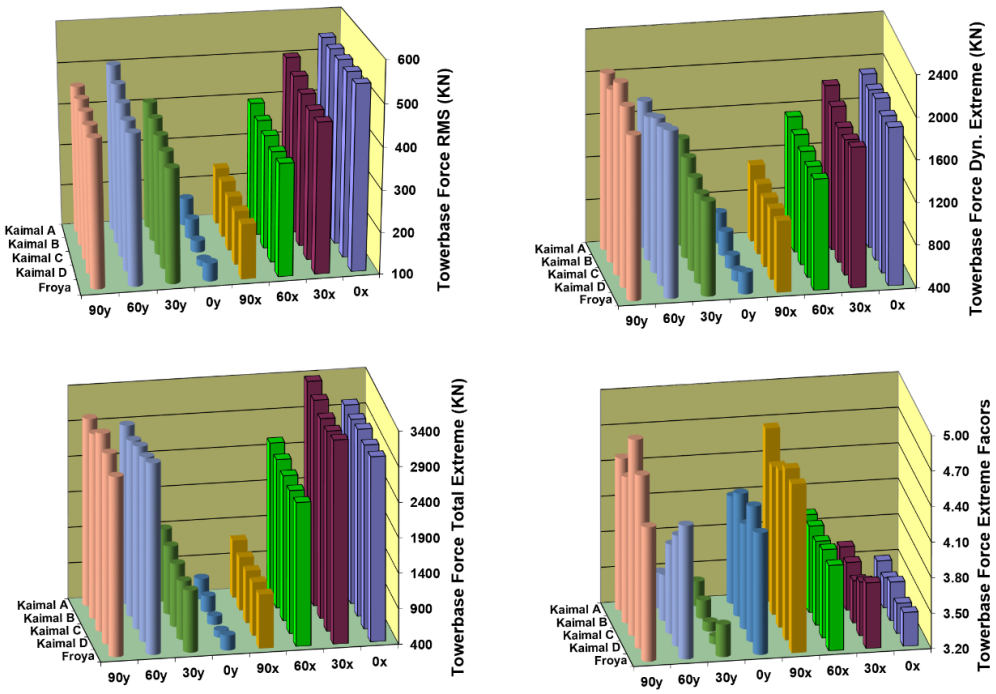

Fig. 25 Statistics of Towerbase Shear Forces – 0, 30, 60 and 90 deg Wind

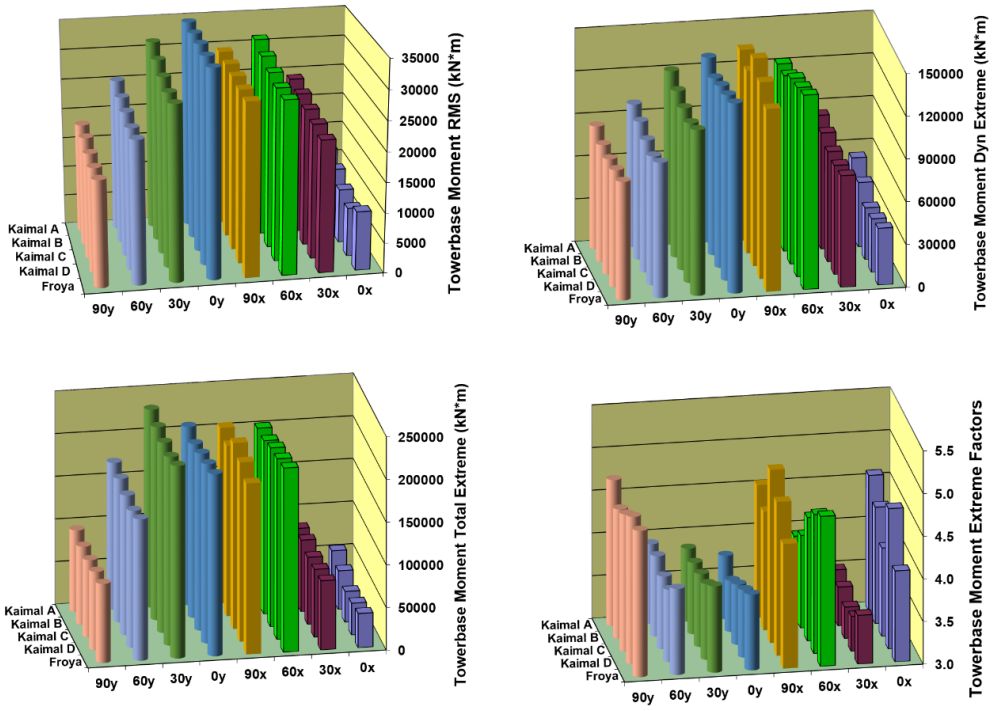

Fig. 26 Statistics of Towerbase Bending Moments – 0, 30, 60 and 90 deg Wind

The effect of wind loading on the system is controlled in large part by the orientation of the blade surfaces relative to the wind's angle of attack, since the tower has a cylindrical cross-section and its exposed area to the wind is the same for every wind heading. It should be noted that the blade pitch used in simulation of the 90 deg wind cases is 75 deg (as mentioned in Section 3.5), which is different from the 90 deg blade pitch used in 0, 30 and 60 deg wind headings. As such, the anomaly (i.e. no variation in weaker responses, per wind spectra type) identified in the shear forces and corresponding bending moments in 90 deg wind heading, are likely due to differences in loading of the blades since the wind acts on a somewhat different exposed area of the blades compared to the 0, 30 and 60 wind heading cases.

5.3 Impact of low frequency dominance of Froya wind velocity

It was emphasized in Section 2 (Fig. 2) that the Froya wind model has more low frequency energy that the Kaimal model. The dominance emphasized in Fig. 2 reflects in the blade root in-plane moments and blade tip deflection, where the Froya moment is higher than the highest Kaimal-induced moment (Fig. 25) at frequency less than 0.01 Hz. In Fig. 25, the outer plots show the energy spectra from 0 to 0.6 Hz; the inner plots or inserts are zoomed plots of each response to delineate energy between 0 and 0.02 Hz. The inner plots clearly show that the Froya model's blade root bending moment energy exceeds the highest Kaimal energy by about 9%, and its blade tip deflection energy exceeds the highest Kaimal energy by about 7%. Blade responses are the only results showing low frequency dominance of the Froya model over all Kaimal models at

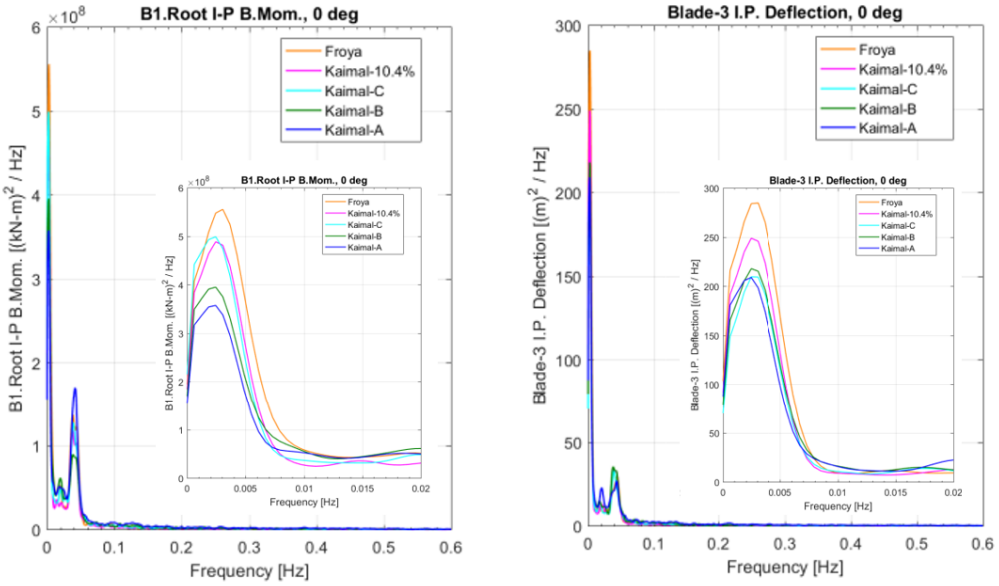

Fig. 27 Spectra of Blade Root In-Plane Bending Moment in 0 deg Wind

frequencies less than 0.01 Hz, akin to that expressed in Fig. 2. Since the blades are directly impacted by the wind loads, it is not surprising that their response spectra are characterized like the wind spectra. It should be noted that two out of the three blades of the turbine show the Froya wind dominance in blade root bending moment and tip deflection, implying that there may be some dependency on the spatial location of the blade for this dominance to manifest.

This observation emphasizes the impact which wind spectrum type can have on RNA design. Although the dynamic extreme responses of the blades (Fig. 11) are not consistently dominated by the Froya model, the exceedance shown in the low frequency region may have significant design consequences on fatigue response, since the spectral energy is a representation of the response RMS. Such potential impacts will be investigated and discussed in Udoh and Zou (in preparation).

5.4 Summary of major findings

Important observations made in the results have led to the following major summary points:

1. Turbulence intensity is not the only important factor to focus on, when considering spectral characteristics of wind models in relation to extreme or strength design of FOWTs. The empirical distribution of wind velocity extremes (upper and lower tails) influence the resulting extreme responses of the system components, depending on wind heading. Two spectral models with the same turbulence intensity but significantly different EDF shapes (as in Kaimal-10.4% and Froya with 10.4% T.I.), will result in different extreme values for design. For several responses (e.g., towerbase Fy in 60 deg), the Froya model produced higher responses (dynamic extremes and extreme

factors) than all Kaimal spectra.

2. A common phenomenon observed in the results is finding that one tail (upper or lower) of the extreme distributions trends with turbulence intensities, and the other indicates no clear trend. This is seen in all components of the system discussed in the results. It is unclear what the controlling factors are, that significantly alter the tail distributions from being correlated with turbulence intensity; however, coupled non-linear interactions between the responses can induce such anomalies in the response trends.
3. It is observed in all coupled responses that the extreme values of dominant response parameters for the different wind spectra, often convergence to almost the same value. Perhaps in the dominant response modes, a 2% differential in the turbulence is not sufficient to drive significant differences in the response. Conversely, the differential in the turbulence intensities is sufficient to delineate significant differences in the weaker response modes. An important point here is that the magnitude of the weaker response(s) relative to the primary response is critical to the overall difference that can be induced by the choice of one wind spectrum over another. In towerbase shear forces in 0 deg, for example, the Kaimal-A Fy force is 35% of its Fx counterpart (which is the dominant shear force) – so the Fy shear makes a significant contribution to the resultant shear force.
4. Many of the characteristics highlighted in the presented results, also exist in the 30 deg and 90 deg responses (most spectra, and extreme distributions not shown). Most of the responses in 30 deg wind heading have similar characteristics to those in the 60 deg wind case, as the oblique wind loads have a similar effect on the different system components. The blade pitch difference of 15 deg (between the 90 deg wind heading cases and those of other headings), seems to have a noticeable effect on the resulting shear forces and bending moments induced at the towerbase.

6. Conclusions

The wind energy industry is now moving rapidly towards offshore developments due to various reasons. However, for FOWTs, so far, there have not been sufficient studies to assess the design implications of selecting wind spectrum models and turbulence intensity curves recommended by the International Electrotechnical Commission (IEC), which are derived from land-based sites and are being widely adopted in offshore wind projects. It is our goal to perform a systematic study of wind spectrum and associated wind turbulence intensity on both strength and fatigue design of offshore wind turbines to meet industry calls.

This paper delineates the governing parameters that influence the extreme loads, regarding wind spectral models for floating offshore wind turbines. The critical factors are turbulence intensity and type of wind spectrum (delineated by their extreme tail distributions). Selection of wind spectra models should be based on their accurate representation of the project site metocean conditions. However, in situations where a model is to be assumed, the combination of spectrum type and turbulence intensity for extreme design should be carefully made to avoid excessively conservative extreme responses. It is important to underscore the fact that the turbulence intensities applied to Kaimal-A, Kaimal-B and Kaimal-C models stem from onshore site studies, and are the current recommended values in the IEC guidelines for wind turbine analysis. Further studies aimed at recommending appropriate turbulence intensity curves for offshore sites are

needed in the industry.

Effects of wind turbulence intensity and type of wind spectrum on fatigue design of FOWTs will be addressed in Udoh and Zou (in preparation).

Acknowledgments

Research described in this paper was funded by Houston Offshore Engineering / Atkins, an SNC-Lavalin company; we express our gratitude to HOE's management for supporting research and development efforts in offshore renewable energy. We acknowledge Hisham Moideen, P.E., for having designed the mooring system for the PC-FWF, and Shobeir Gar, Ph.D., P.E., for generating the structural scantling and weights used in analysis, as well as the mesh model shown in Fig. 4.

References

Anderson, O.J. and J. LØvseth (1992), "The maritime turbulent wind field. measurements and models", Final Report for Task 4 of the Statoil Joint Industry Project, Norwegian Institute of Science and Technology, Trondheim, Norway.

Anderson, O.J. and LØ vseth, J. (2006), "The FrØya Database and Maritime Boundary Layer Wind Description", *Mar. Struct.*, **19**, 73-192.

Bagbanci, H. (2011), "Dynamic analysis of offshore floating wind turbines", Master's Degree Dissertation, Technical University of Lisbon (Instituto Superior Técnico, Universidade Técnica de Lisboa), Portugal.

Bir, G. (2005), "User's Guide to BMODES (Software for Computing Rotating Beam Coupled Modes)", Technical Report, National Renewable Energy Laboratory, NREL/TP-500-39133, Golden CO. USA.

Det Norske Veritas (2007), Recommended Practice DNV-RP-C205, *Environmental Conditions and Environmental Loads*, 19-20.

Elsayed, A.E. (2012), *Reliability Engineering*, John Wiley and Sons, Hoboken, New Jersey, USA.

International Electrotechnical Commission (2005), IEC 61400-1, *International Standard on Wind Turbines, Part 1: Design Requirements*, Third Edition, 1301-1328.

International Electrotechnical Commission (2009), IEC 61400-3 (BS EN 61400-3), *International Standard on Wind Turbines, Part 3: Design Requirements for Offshore Wind Turbines*.

Jonkman, B.J. and Buhl, M.L., Jr. (2005), "FAST User's Guide", Technical Report, National Renewable Energy Laboratory, NREL/TP-500-38230, Golden CO. USA.

Jonkman, B.J. and Kilcher, L. (2012), "Turbsim user's guide", Technical Report, National Renewable Energy Laboratory, Golden CO. USA.

Jonkman, J. (2007), "Dynamic modeling and loads analysis of an offshore floating wind turbine", Technical Report, National Renewable Energy Laboratory, NREL/TP-500-41958, Golden CO. USA.

Jonkman, J. Butterfield S., Musial, W. and Scott, G. (2009), "Definition of a 5-MW reference wind turbine for offshore system development", Technical Report, National Renewable Energy Laboratory, NREL/TP-500-38060, Golden CO. USA.

Kaimal, J.C., Wyngaard, J.C., Haugen, D.A., Cote, O.R. and Izumi, Y. (1976), "Turbulence structure in the convective boundary layer", *J. Atmop. Sciences*, **33**(417), 2152-2169.

Kaimal, J.C., Wyngaard, J.C., Izumi, Y. and Cote, O.R. (1972), "Spectral Characteristics of Surface-layer Turbulence", *J. Roy. Meteorol. Soc.*, **98(**417), 563-589.

Maritime Research Institute Netherlands (2007), "Wind Loads on Offshore Structures (WINDOS), User Guide for WINDOS Engineering Tool".

Masciola, M., Robertson A., Jonkman, J. and Driscoll, F. (2011), "Investigation of a FAST-OrcaFlex

Coupling Module for Integrating Turbine and Mooring Dynamics of Offshore Floating Structures", National Renewable Energy Laboratory, NREL/CP-5000-52896, Golden CO. USA.

Orcina Ltd., OrcaFlex User Manual, version 9.7, www.orcina.com.

Tong, W. (2010), *Wind Power Generation and Wind Turbine Design*, WIT Press, Billerica, Massachusetts, USA.

Udoh, I.E. and Zou, J. (2016), "Wind turbulence effects in global responses of a 5 MW wind turbine TLP", *Proceedings of the 21ST Offshore Symposium – Texas Section of the Society of Naval Architects and Marine Engineers*, Houston, USA, February.

Udoh, I.E. and Zou, J. (In Preparation), "Wind Spectra Characteristics on Fatigue Design of Floating Offshore Wind Turbines".

Udoh, I.E., Zou, J. and Edgar, C. (2016), "Impacts of wind turbulence on the performances of s semi-submersible type and TLP-type wind turbine", *Proceedings of the Offshore Technology Conference*, OTC-27261-MS, Houston, USA, May.

WAMIT Inc. (2006), WAMIT User Manual, version 6.4, Massachusetts Institute of Technology and www.wamit.com.

Mk